



NJC

**Killing Two Birds with One Stone: Phosphorylation by a Tabun Mimic and Subsequent Capture of Cyanide Using a Single Fluorescent Chemodosimeter**

Journal:	<i>New Journal of Chemistry</i>
Manuscript ID	NJ-ART-08-2022-004014.R2
Article Type:	Paper
Date Submitted by the Author:	18-Oct-2022
Complete List of Authors:	Mia, Rashid; The University of Southern Mississippi, Chemistry and Biochemistry Cragg, Peter; University of Brighton, School of Pharmacy and Biomolecular Sciences Fronczek, Frank; Louisiana State University, Chemistry Dept Wallace, Karl; The University of Southern Mississippi, Chemistry and Biochemistry

SCHOLARONE™  
Manuscripts

## ARTICLE

# Killing Two Birds with One Stone: Phosphorylation by a Tabun Mimic and Subsequent Capture of Cyanide Using a Single Fluorescent Chemodosimeter

Received 00th January 20xx,  
Accepted 00th January 20xx

DOI: 10.1039/x0xx00000x

Rashid Mia,<sup>a</sup> Peter J. Cragg<sup>b</sup>, Frank R. Fronczek,<sup>c</sup> and Karl J. Wallace\*<sup>a</sup>

**ABSTRACT:** In the presence of the tabun mimic diethylcyanophosphonate (DECP), a fluorescent bifunctional coumarin-enamine chemodosimeter is first phosphorylated and subsequently attacked by the released cyanide ions. The reaction is disclosed in both the UV-vis and fluorescence spectra and confirmed by NMR experiments. DFT calculations support that the *bis*-adduct as the most thermodynamically stable species. The X-ray structure of the chemodosimeter is also reported.

## Introduction

Simultaneous recognition of ion pairs has been documented for over 30 years.<sup>1</sup> It can be achieved by tweezer type heteroditopic receptors, for example, those based on the 2-pyridyl-acylhydrazone framework, that acts as a photoswitch<sup>2</sup> and bowl shaped molecules, for examples those derived from calix[n]arenes<sup>3</sup>, cavitands<sup>4, 5</sup>, pillar[n]arenes<sup>6</sup>, and cascade receptors<sup>7</sup>, in which ion pairs are bound separately either within, or outside, the cavity of a bifunctional host molecule by complementarity recognition motifs. Additional other charged species, such as zwitterions, have been shown to bind within the cavity of cyclodextrins.<sup>8</sup>

The use of fluorescent probes as bifunctional chemodosimeters is less well explored and is an attractive approach to target analytes where a bifunctional approach can improve selectivity. Organophosphate molecules are ideal targets for chemodosimeters as many such probes contain nucleophilic moieties that can phosphorylate the electrophilic centre of the organophosphate.<sup>26</sup> Phosphorylation can cause either distinctive colorimetric or emission changes through fluorescent mechanisms such as PET, ESIPT, ICT and intramolecular cyclization mechanisms.<sup>9</sup> All of these have been employed in molecular probe designs through the introduction of nucleophiles, that have been incorporated onto an organic backbone, a metal ion or a polymer, such as hydroxyl<sup>10-18</sup>, pyridine<sup>19, 20</sup>, amine<sup>21</sup> and oximate<sup>22, 23</sup> groups, to trigger a

fluorescent response to organophosphates and F<sup>-</sup><sup>21</sup> and CN<sup>-</sup>.<sup>24, 25</sup>

As part of our ongoing research on the design and synthesis of molecular probes for nerve agent detection, we have incorporated the coumarin-enamine motif to act as a bifunctional molecular chemodosimeter to target diethylcyanophosphonate (DECP), a tabun mimic. We have shown that it can act as a triggering agent (oxime moiety) that is phosphorylated by the tabun mimic before capturing the liberated CN<sup>-</sup> leaving group by enamine moiety on a single organic platform. In this context, very few bifunctional compounds have been developed: the authors are aware of a fluorescent fluorescein derivative<sup>10, 26</sup> and a BODIPY molecule that can distinguish tabun and sarin mimics but these are used predominantly as colorimetric sensors.<sup>16</sup> Even though colorimetric sensing through naked-eye recognition is an attractive approach it is not as sensitive as fluorescence-based chemodosimetry as the former is only as sensitive as the observer's eyes. To the best of our knowledge, this is the first coumarin derived molecule that offers a dual mechanism in its fluorescent response. Despite the attractiveness of using a single molecule to target nerve agents, there are drawbacks. Tabun is unique among the G-series in that it contains a phosphorous-nitrile bond (Fig. 1) while sarin, cyclosarin, and soman have a phosphorous-fluoride bond. While this limits the broader use of the coumarin-enamine system, it does provide a highly selective probe.

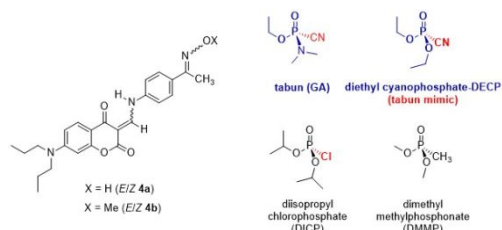


Fig. 1. Chemodosimeter **4a**, Tabun and nerve agent mimics.

<sup>a</sup> Department of Chemistry and Biochemistry, The University of Southern Mississippi, Hattiesburg, MS 39406, United States Address here.

<sup>b</sup> School of Pharmacy and Biomedical Sciences, University of Brighton, Brighton BN2 4GJ, UK

<sup>c</sup> Department of Chemistry, Louisiana State University, Baton Rouge, LA 70803, United States

† Electronic Supplementary Information (ESI) available: 1D and 2D NMR, optical studies, Solid state structures and Tables, ESI-MS and modelling See DOI: 10.1039/x0xx00000x

## Results and discussion

### Design, Synthesis, and Crystallography Studies

The coumarin-enamine scaffold is a very versatile organic framework that can be easily derivatised in different positions. This allows us to design an organic molecular probe that can incorporate diverse functional groups, thus taking advantage of different fluorescent mechanisms. For example, the fluorescence of the ketoxime/ketoximate is initially quenched by a PET mechanism, which turns back on upon the formation of the adduct. It therefore performs as an “off-on” sensor which switches between hypochromic and hyperchromic shifts. A moiety capable of undergoing the ESIPT mechanism to shift the wavelength further in the hypsochromic direction was also incorporated into the molecular design.

Chemodosimeter **4a** was successfully synthesized in a few steps (Scheme S1, ESI†). The NMR spectra show both geometric isomers are observed in a 3:1 ratio of *E*-(*keto*) enamine-*anti*-ketoxime and *Z*-(*keto*) enamine-*anti*-ketoxime respectively (Table S1 and Fig. S1-15, ESI†). X-Ray quality crystals of the thermodynamically stable *E*-(*keto*) enamine-*anti*-ketoxime (**4a**), were obtained from a concentrated DMSO solution. Compound **4a** is planar, stabilised by the resonance assisted hydrogen bonding (RAHB) interaction S(6) motif which, together with its extensive conjugation, gives rise to the optical properties observed. The crystal packing is dominated by hydrogen bonding between the oxime moiety of one molecule and the *keto* functional group of a molecule related by an inversion center in an *anti*-orientation, forming a  $R_1^2(22)$  ring system, which also contains the S(6) motif (Fig. 2 and Fig. S16, ESI†).<sup>27</sup>

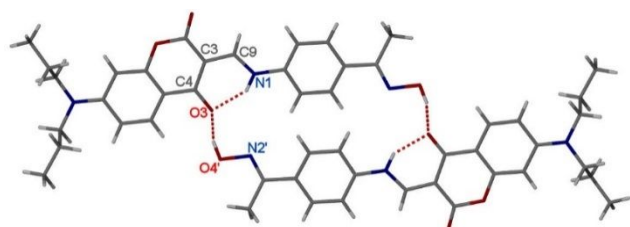
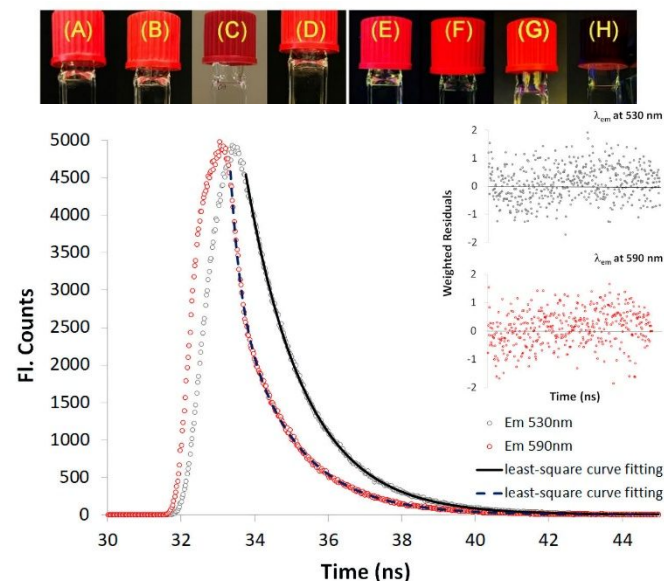


**Fig 2.** Crystal structure of **4a**, illustrating the two unique hydrogen bond interactions (dashed lines). One intramolecular interaction with a donor-acceptor distance; N(1)-H(1)N $\cdots$ O3 = 2.626(5) and another intermolecular interaction O4'-H $\cdots$ O3 = 2.707(5).

### Photophysical Studies

### UV-vis, Steady state, and fluorescent lifetime: We recently



reported an example of a coumarin-enamine with a fluorescence quantum yield of  $\phi = 0.83$ .<sup>28</sup> We found no evidence of tautomers for **4a** in the NMR study but they could be identified using fluorescence life-time studies. Consequently, the existence of different tautomers in **4a** was investigated through its fluorescence lifetime decay. Four different excited state-species were confirmed in DMSO ( $2.0 \mu\text{mol}\cdot\text{dm}^{-3}$ ) by measuring decay profiles both at a high-energy emission ( $\lambda_{\text{em}} = 530 \text{ nm}$ ) and low-energy emission ( $\lambda_{\text{em}} = 590 \text{ nm}$ ) (Fig. 3). Both spectral features were fitted with a double exponential function confirming that two tautomeric species are present for each geometric isomer in solution. The high-energy emission was calculated to have  $\tau = 0.81 \text{ ns}$  (4%) and  $1.57 \text{ ns}$  (96%) whereas the low-energy emission gave  $\tau = 0.25 \text{ ns}$  (36%) and  $1.6 \text{ ns}$  (64%) (Table S2, ESI†).<sup>29</sup>

**Fig 3.** The fluorescence lifetime of **4a** ( $2.0 \mu\text{mol}\cdot\text{dm}^{-3}$ , DMSO); Insert weighted residuals at  $\lambda_{\text{em}} = 530 \text{ nm}$  (insert-top) and  $590 \text{ nm}$  (insert-bottom) confirming the existence of four tautomers using  $300 \text{ nm}$  NanoLED LESER light source ( $298 \text{ K}$ ).

The next step was to form the ketoximate through the addition of base. Here, a non-nucleophilic base was required to abstract the proton from the oxime moiety without itself undergoing nucleophilic addition to the organophosphate. Potential non-nucleophilic bases include the phosphazene class of superbases such as  $\text{P}_4\text{-}t\text{-Bu}$  (MeCN  $\text{pK}_{\text{aH}} = 42.7$ , or 1,8-diazabicyclo [5.4.0] undec-7-ene (DBU; MeCN  $\text{pK}_{\text{aH}} = 24.3$ ) or  $\text{N,N}$ -diisopropylethylamine (Hünig’s base; MeCN  $\text{pK}_{\text{aH}} = 18.1$ ).<sup>30, 31</sup> The particular base and the amount used are crucial and careful control is required. The coumarin-enamine scaffold contains the RAHB motif necessary to make the compound highly fluorescent. If deprotonation of the RAHB occurred the optical studies will be perturbed, rendering the fluorescence signal worthless. Additionally, nerve agent mimics are notoriously acidic, containing trace amounts of acid even when purchased fresh. It was determined that ten equivalents of  $\text{P}_4\text{-}t\text{-Bu}$  base was optimal to form the ketoximate without disrupting the RAHB<sup>28</sup> while also reacting with the excess acid

in the solution of DECP. The instantaneous color change<sup>32, 33</sup> can be observed with the naked eye, and the fluorescence signature is very different under UV, Fig 4.

**Fig 4.** (A and E) Probe ( $16 \mu\text{mol}\cdot\text{dm}^{-3}$ , DMSO) (B and F) **4a** plus three equivalents of KCN, (C and G) **4a** plus ten equivalents of  $\text{P}_4\text{-t-Bu}$  and (D and H) **4a**-ketoximate plus three equivalents of DECP; long wavelength (366 nm).

Upon the addition of  $\text{P}_4\text{-t-Bu}$  base the band hypsochromically shifted to 374 nm. Upon titrating nine equivalents of DECP to **4a**-ketoximate the band at 374 nm decreased in intensity with the appearance of two distinctive bands at 327 nm and 411 nm (Fig. Fig. 5A) Deconvoluting the UV-vis spectrum reveals two clear and distinctive UV-vis spectra both showing two distinctive processes occurring (Fig. S17, ESI<sup>†</sup>). When the absorbance ratio at 326/374 and 411/374 nm are plotted

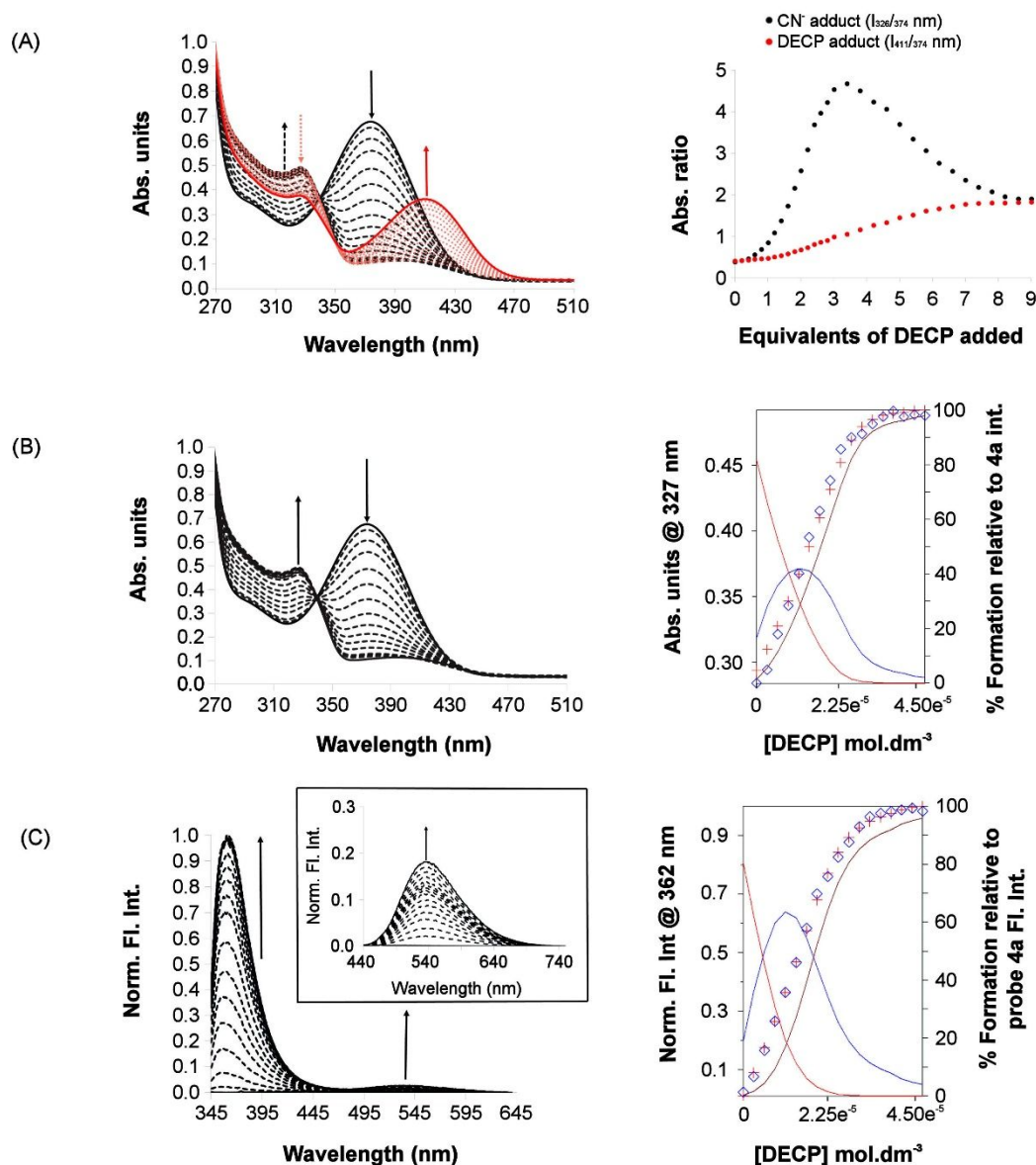
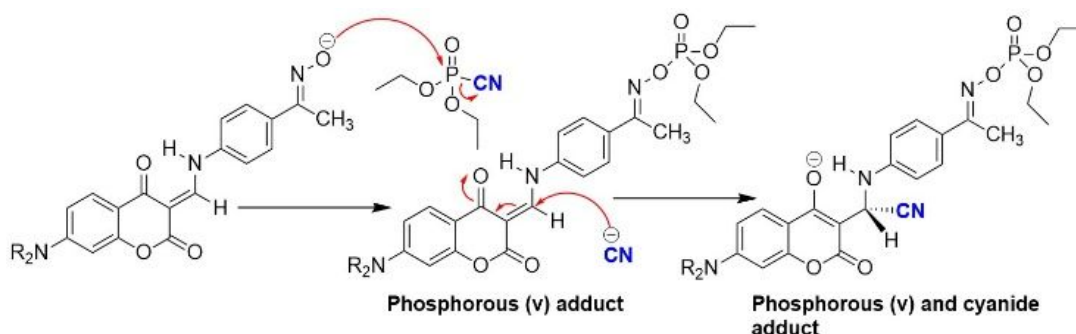


**Fig 5.** The UV-vis and emission spectra of **4a**-ketoximate ( $16 \mu\text{mol}\cdot\text{dm}^{-3}$ , DMSO) (A) UV-vis spectra on the adduct of aliquots of 0-9 equivalents, DECP (B) The deconvoluted UV-vis and binding data, (C) fluorescence spectra on the addition of aliquots of 0-3 equivalents DECP ( $\lambda_{\text{ex}} = 336 \text{ nm}$  and insert ( $\lambda_{\text{ex}} = 410 \text{ nm}$ ) (and) the fluorescence binding data. Blue diamonds: experimental data; red crosses: fitted data using HypSpec<sup>™</sup>. Coloured solid lines highlight fitting to 1:1 and 2:1 species.

A UV-vis experiment was carried out by preparing a  $16 \mu\text{mol}\cdot\text{dm}^{-3}$  solution of **4a** in DMSO, which produced a featureless absorption band with a  $\lambda_{\text{max}}$  observed at 413 nm.

against equivalents the two binding isotherms obtained do not represent a traditional 1:1 or 2:1 binding isotherm (Fig 5A). However, upon the inspection of the binding behaviour at the lower concentrations of up to 3 equivalents, the binding



**Scheme 1** . Proposed bis-adduct formed upon phosphorylation of DECP at the lower concentration range of the titration (up to the addition of three equivalents of DECP added); R = propyl.

isotherms are resolved with saturation occurring at 3 equivalents (Fig 5B CN<sup>-</sup> adduct shown)). The UV-vis isotherm shows a sigmoidal binding behaviour indicative of 2:1 binding. The fluorescence spectra show an increase in both the *keto*\* emission band and the band at 361 nm (Fig 5C and Fig. S19-21, ESI<sup>+</sup>). The fluorescence binding behaviour mirrors the UV-vis data. Using non-linear regression to fit all of the data (0 to 9 equivalents) was a challenge and no reasonable thermodynamic data were obtained. However, at lower concentrations of 0 to 3 equivalents, the titration profile can be fitted to both a 1:1 and 2:1 model using non-linear regression (Fig. 5C-HypSpec; Protonic Software).<sup>34</sup> Using the emission data the log  $K_{11}$  and log  $K_{12}$  were calculated to be 6.92(4) M<sup>-1</sup> and 5.82(1) M<sup>-1</sup>, respectively. Phosphorylation occurs initially, this is best seen in the emission spectra whereby the PET mechanism is switched on upon the initial additions of DECP (Fig S21, ESI<sup>+</sup>), once enough cyanide ions have been liberated, the emission band at 361 increases in intensity as the CN<sup>-</sup> ion undergoes Michael addition on the enamine moiety (see NMR discussion). This adduct produces a distinctive absorption band at 327 nm (Fig. 5B) and a strong emission band at 361 nm (Fig. 5C). This is due to the Michael addition disrupting the conjugation as the molecule undertakes a drastic structural change. The proposed *bis*-adduct, depicted in Scheme 1, correlates with the organic framework change (*vide infra*) and the absorbance and emission changes observed.

To confirm the *bis*-adduct, we carried out a series of model studies with KCN, diisopropylchlorophosphate (DICP) and dimethyl methylphosphonate (DMMP). In UV-vis studies, initially, aliquots of KCN were added into a 16 μmol·dm<sup>-3</sup> solution **4a** containing no base. A band at 412 nm decreased and a new band at 327 nm appears with an isosbestic point at 352 nm (Fig. S18A, ESI<sup>+</sup>). This is in excellent agreement with the appearance of the band due to the formation of the CN<sup>-</sup>-adduct on the addition of DECP as described above. Other anions are less likely to undergo a Michael addition<sup>32</sup> therefore, we added DICP, a chloride-containing organophosphate. After phosphorylation, a band at 412 nm appears with an isosbestic point 389 nm, in agreement with the other phosphorylation reactions, but no additional UV-vis bands were observed where

those from the Michael adduct would be expected (Fig. S18C, ESI<sup>+</sup>). DMMP is not prone to phosphorylation (Fig. S22E, ESI<sup>+</sup>) due to the poor -CH<sub>3</sub> leaving group and, consequently, the absorption band at 412 nm did not change. Additionally, we also synthesized compound **4b** and repeated the UV-vis studies described above. The addition of DICP, DMMP and DECP did not yield any further spectral change (Fig. S18, ESI<sup>+</sup>). However, upon the addition of KCN to **4b** a band at 326 nm appears, further supporting the formation of the CN<sup>-</sup> adduct (Fig. S18B, ESI<sup>+</sup>)

Due to sequential phosphorylation and capture of the CN<sup>-</sup> ion it was anticipated that a steady-state fluorescence spectrum would be observed. A 16 μmol·dm<sup>-3</sup> solution of **4a** in DMSO ( $\lambda_{\text{ex}} = 336$  nm) was prepared. On the addition of ten equivalents of P<sub>4</sub>-*t*-Bu base the ketoximate is formed and PET quenches the fluorescence signal; upon phosphorylation the fluorescence signal is re-established. When DECP ( $\lambda_{\text{ex}} = 336$  nm) is added a dual-channel emission is observed with bands at 537 nm and 361 nm which were assigned to the phosphorylated and Michael addition *bis*-adduct (Fig. 5 and Fig. S19, ESI<sup>+</sup>). The dual-channel emissions were supported by analogous control experiments to those used in the UV-vis investigation. Addition of aliquots of KCN support the observation that the fluorescence enhancement seen at 361 nm and quenching at 537 nm was due to the formation of the CN<sup>-</sup> adduct (Fig. S22, ESI<sup>+</sup>). The addition of DICP and DMMP caused no fluorescence changes at 361 nm (Fig. S22, ESI<sup>+</sup>). However, DICP did show a strong fluorescence emission enhancement at 537 nm due to phosphorylation, as expected (Fig. S22, ESI<sup>+</sup>). No spectral changes due to phosphorylation were observed under the same conditions for the methylated analogue, **4b** (Fig. S23, ESI<sup>+</sup>). Addition of KCN had the same effect on the bands at 361 nm and 537 nm indicating formation of the CN<sup>-</sup> adduct (Fig. S23A, ESI<sup>+</sup>). DECP and DICP showed fluorescence enhancement at 397 nm due to the presence of trace HCN and HCl found even in freshly purchased DECP and DICP, respectively (Fig. S23, ESI<sup>+</sup>). To overcome this problem, we added base into the analyte solution before the experiments were carried out to prevent false positives. Thus, the spectrochemical response observed is solely from the formation of the adduct.

The fluorescence lifetime decay profiles of **4a** were shown to have a number of excited state species as a consequence of different tautomers in solution (*vide supra*). These do not exist when DECP is added to the solution so the decay profiles should be significantly different, (Fig. 6). The lifetime ( $\tau$ ) was 1.61 ns for **4a** whereas for the ketoximate it was 2.28 ns due to a PET mechanism. This was found to be a double exponential fit with a rapid first decay profile calculated to be 870 ps due to the lone pair on the ketoximate ion. The second decay was significantly longer at 6.20 ns due to non-radiative decay (Table 1). The excited state can be depopulated rapidly upon phosphorylation by DECP or DIPC ( $\tau = \sim 1.60$  ns) whereas DMMP shows no significant changes, as it cannot phosphorylate. KCN can still react and disrupt RAHB conjugation (Fig. S24, ESI<sup>†</sup>). The methylated analogue **4b** shows no lifetime changes with DECP, DIPC and DMMP as it cannot form the ketoximate ( $\tau = 1.64$  ns) (Fig. S25, ESI<sup>†</sup>). As expected, it is affected by KCN ( $\tau = 2.14$  ns; Table S3, ESI) as the Michael addition of CN<sup>-</sup> can still occur and disrupt RAHB conjugation.

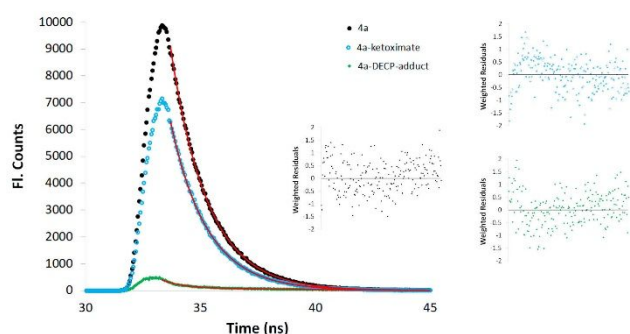


**Fig 6.** Fluorescence lifetime of **4a**-ketoxime, **4a**-ketoximate ( $16.00 \mu\text{mol}\cdot\text{dm}^{-3}$ , DMSO,  $\lambda_{\text{em}} = 540$  nm, 298 K) and upon the addition of DECP; insert weight residuals. using 300 nm LESER light source.

**Table 1.** Fluorescence lifetime of **4a**-ketoxime, **4a**-ketoximate ( $16.00 \mu\text{mol}\cdot\text{dm}^{-3}$ , DMSO,  $\lambda_{\text{em}} = 540$  nm, 298 K) and upon the addition of DECP, KCN, DIPC, DMMP using 300 nm LESER light source.

		$\tau_1$ (ns) (3 $\sigma$ )	$\tau_2$ (ns) (3 $\sigma$ )	$\bar{\tau}$ (ns) (3 $\sigma$ )	A (3 $\sigma$ )	$\chi^2$
<b>4a</b>	Run 1	1.61(1)	-	-	2.86(7)	1.07
	Run 2	1.61(1)	-	-	2.86(5)	1.07
<b>4a-ketoximate</b>	Run 1	0.86(2)	6.28(5)	2.24(5)	2.43(3)	1.19
	Run 2	0.878(2)	6.12(5)	2.32(5)	5.07(4)	1.14
<b>4a-adduct</b>	Run 1	0.159(2)	9.23(1)	1.6(1)	1.44(4)	1.13
	Run 2	0.159(2)	8.54(8)	1.6(4)	0.866(4)	1.05

As both the phosphorous adduct and the CN<sup>-</sup>-adduct are distinguishable in the fluorescence spectra, emission bands can be used to determine the limit of detection (LOD) of the Tabun mimic. For chemodosimeter **4a** these were calculated to be 11 ppb ( $12.2 \mu\text{g}\cdot\text{m}^{-3}$ ) and 24 ppb ( $24 \mu\text{g}\cdot\text{kg}^{-1}$ ), using the CN<sup>-</sup> ion and phosphate adduct respectively (Fig. S43, ESI<sup>†</sup>), significantly lower than limits found in the literature (CN<sup>-</sup>  $5 \text{ mg}\cdot\text{m}^{-3}$ )<sup>35</sup> and tabun ( $\text{LD}_{50} = 14.3 \text{ mg}\cdot\text{kg}^{-1}$ ).<sup>36</sup>

### NMR and Mass Spectrometry Studies

To confirm that the spectroscopic response was due to bifunctional binding, we investigated the structural changes by 1D and 2D proton NMR and carbon-13 NMR, and phosphorus-31 NMR, which showed that **4a** exists as geometrical isomers (Table S1, ESI<sup>†</sup>). These isomers disappear upon the addition of DECP as the CN<sup>-</sup> ion undergoes a 1,4-Michael addition thereby changing the hybridization of C9 from  $sp^2$  to  $sp^3$  as observed in both the <sup>1</sup>H (Fig. 7) and <sup>13</sup>C APT spectra (Fig 7). As the NMR experiments were carried out in the millimolar range, rather than micromolar concentration used for the spectroscopic studies, the experimental conditions had to be subtly changed as P<sub>4</sub>-t-Bu would deprotonate the hydrogen atom that participates in the RAHB motif at this higher concentration. Therefore, Hünig's base was used to ensure the RAHB motif remained in the organic framework.

The <sup>1</sup>H NMR of **4a** ( $20 \text{ mmol}\cdot\text{dm}^{-3}$ ) shows two distinct doublets at  $\delta$  13.52 and 11.59 ppm assigned to the geometric isomers E(NH) and Z(NH) respectively (Fig. S1, ESI<sup>†</sup>). This was confirmed by HSQC as no correlation was seen with any carbon atom and the signals disappear when D<sub>2</sub>O is added. Upon the addition of KCN, the spectrum was significantly different as the isomers were lost. Both proton signals disappeared, and a new sharp doublet appeared up-field at  $\delta$  6.39 ppm, assigned to the NH signal (Table S4 and Fig. S26-36, ESI<sup>†</sup>). Following the addition of DECP the NH signal appears at  $\delta$  6.40 ppm (Fig. 7(top)) due to hybridization changes of  $sp^2$  C(9)H ( $E = \delta$  8.77,  $Z = \delta$  8.81 ppm, to  $sp^3$  ( $\delta = 5.64$  for KCN addition,  $\delta = 5.65$  for DECP addition) (see NMR spectra, ESI<sup>†</sup>). The <sup>13</sup>C APT spectrum supported the <sup>1</sup>H NMR as the enamine moiety carbons C(3) and C(9), observed at  $E = \delta$  97.5,  $Z = \delta$  97.8 ppm (Fig. 7) and  $E = \delta$  153.3,  $Z = \delta$  151.8 ppm (Fig. 7) respectively, shifted upfield to 88.4 and 40.6 ppm following both KCN and DECP addition. Furthermore, in both additions the cyanide carbon was observed at 120.6 ppm in the APT negative mode (Fig. 7).

Organophosphates have a phosphorous (V) centre which makes <sup>31</sup>P NMR experiments an excellent diagnostic tool to investigate the phosphorous chemical environment of the adduct. The **4a**-ketoximate-DECP adduct generated three signals at  $\delta$  -21.30, -13.30 and -0.95 ppm. In the <sup>31</sup>P NMR spectrum of DECP, where  $\delta$  -21.30 ppm corresponded to DECP,  $\delta$  -13.30 and -0.95 ppm were assigned as the phosphate dimer and diethyl phosphoric acid, respectively (Fig 7).<sup>37, 38</sup> Upon the addition of one equivalent of DECP to **4a**-ketoximate ( $20 \text{ mmol}\cdot\text{dm}^{-3}$ ) all signals disappeared. A new signal appeared at -0.64 and assigned to the [**4a**-DECP] adduct that confirmed phosphorylation had taken place, consistent with the literature.<sup>37</sup>

The existence of the phosphorylated product and phosphorylated CN<sup>-</sup>-adduct were also confirmed by ESI-MS from the  $m/z$  of 607.3 [(**4a**+DECP)+Na]<sup>+</sup> for both phosphorous (V) species (Fig. S42, ESI<sup>†</sup>). The free ligand [**4a**-H]<sup>-</sup> was seen at 420.1 (Fig. S40-S42, ESI<sup>†</sup>) and its sodium adduct, [**4a**+Na]<sup>+</sup>, at 444.2. Upon the addition of KCN to **4a**, [**4a**+CN]<sup>-</sup> is observed at 446.9 (negative mode) (Fig. S41, ESI<sup>†</sup>).

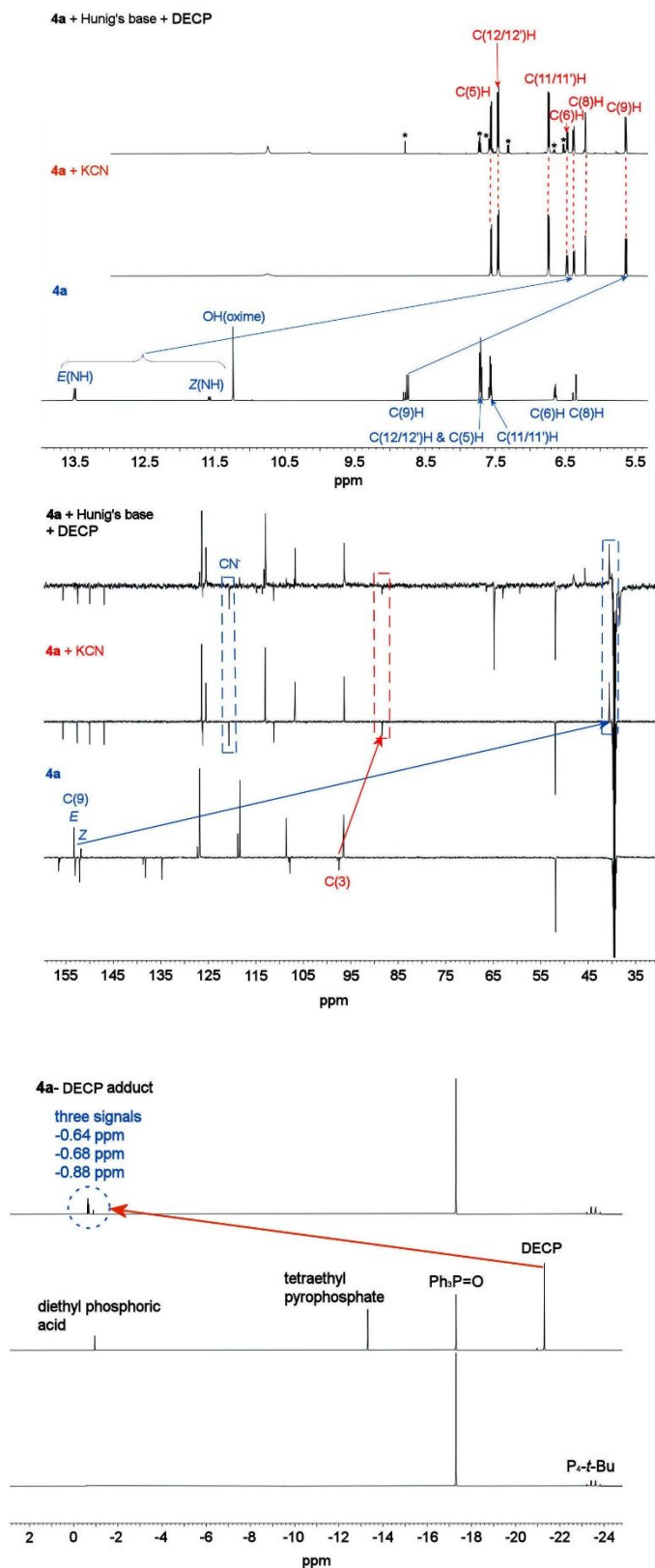


**Fig 7. Top:** Partial  $^1\text{H}$  NMR spectra showing the change of **4a** upon the addition of KCN and DECP (**4a** only, **4a** plus two equivalents KCN, **4a-ketoximate** plus three equivalents of DECP \* degraded products) **Middle:**  $^{13}\text{C}$  APT spectra showing the change of **4a** upon the addition of KCN and DECP (**4a** only, **4a** plus two equivalents of KCN to observe Michael-addition of  $\text{CN}^-$ , **4a-ketoximate** plus three equivalents of DECP to observe the Michael-addition product of phosphorylated  $\text{CN}^-$  ions. **Bottom:**  $^{31}\text{P}$  NMR spectra (242.9 MHz, decoupling) of  $\text{P}_4\text{-t-Bu}$  alone, addition of DECP, **4a-ketoximate** plus one equivalence DECP; a capillary tube containing triphenyl phosphate was used as the internal standard (20  $\text{mmol}\cdot\text{dm}^{-3}$  in DMSO at 298 K.

### Modelling Studies

We have previously shown that cyanide addition can only occur at C(9) on the *E*-(keto) enamine-anti-ketoxime isomer.<sup>32</sup> Therefore, we investigated a reaction scheme computationally. Reactant, product, and transition state structures were calculated by the following DFT basis set  $\omega\text{B97X-D/6-31G}^*$ . Following initial reaction, the pathway was downhill to form the most thermodynamically favourable bis-adduct product. The final gas phase structure (Fig. 8) seems to be stabilized by hydrophobic interactions between one of the ethyl groups of the tabun mimic and the “cavity” formed as the molecular probe seems to bend in on itself.

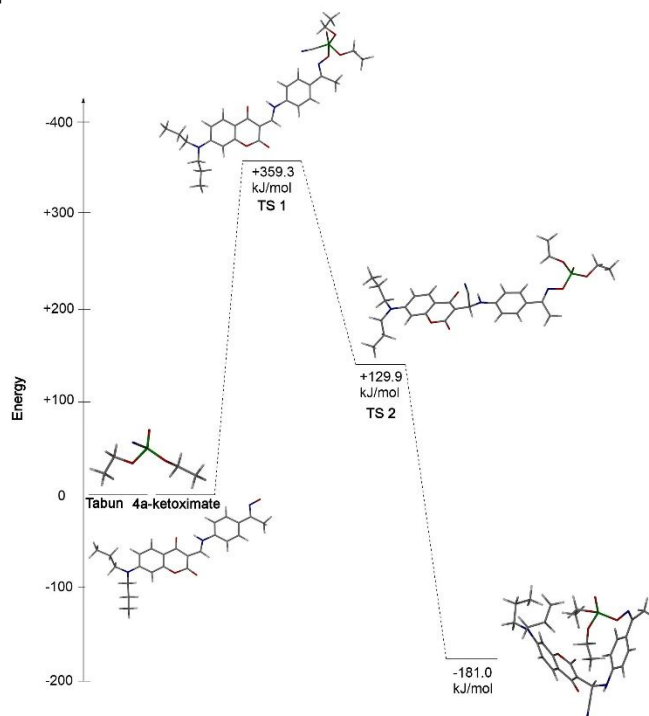


**Fig 8.** The reaction pathway and minimized DFT calculation showing the thermodynamically stable bis-adduct formation.

### Conclusion

In summary, a bifunctional chemodosimeter, **4a**, based on a coumarin-enamine scaffold, has been synthesised and shown to concurrently trigger phosphorylation of an organophosphate tabun mimic, DECP, and capture of the CN<sup>-</sup> ion that has been released. The structure of the chemodosimeter in its *E*-(*keto*) enamine-*anti*-ketoxime form was confirmed by X-ray crystallography. Four fluorescent species were observed in solution corresponding to the two tautomers of each geometric isomer. The reaction between the oxime form of probe **4a** and DECP demonstrated both phosphorylation, through changes in UV-vis absorbance ratios at 326/374 nm and 411/374 nm, and CN<sup>-</sup> attack through the appearance of a new peak at 327 nm. A combination of spectroscopic and spectrometric studies showed that addition of KCN alone only generates the CN<sup>-</sup>-adduct whereas reaction with diisopropylchlorophosphate (DICP) only causes phosphorylation as the liberated Cl<sup>-</sup> cannot undergo a Michael addition. Consequently, **4a** performs as a highly selective chemodosimeter for organophosphates incorporating cyanide moieties.

## Experimental

### General techniques

One-dimensional <sup>1</sup>H, and <sup>13</sup>C NMR spectra and two-dimensional NMR (HMBC and HSQC) were recorded on a Bruker Avance 400 or 600 spectrometer operating at a proton frequency of 400.13 MHz or 600.13 MHz, both equipped with a standard BFO 5 mm two-channel probe in the appropriate deuterated solvents. Chemical shifts are reported in parts per million (ppm) downfield from tetramethylsilane (0 ppm) as the internal standard and coupling constants (J) are recorded in hertz (Hz). The multiplicities in the <sup>1</sup>H NMR spectra are reported as (br) broad, (s) singlet, (d) doublet, (dd) doublet of doublets, (t) triplet, (sx) sextet and (m) multiplet. All spectra were recorded at ambient temperature unless otherwise stated. Low resolution mass spectra were measured with Finnigan TSQ70. High-resolution mass spectra (HRMS) analysis was completed using positive or negative ion-mode electrospray ionization (ESI) with an Apollo II ion source on a Bruker 10T Apex-Qe FTICR-MS recorded at Old Dominion University. IR spectra were obtained on a Nicolet Summit FT-IR paired with a Smart Orbit ATR attachment. The characteristic functional groups are reported in wavenumbers (cm<sup>-1</sup>) and are described as weak (w), medium (m), strong (s), and very strong (vs). UV-Vis experiments were carried out on an Evolution 220 UV-vis spectrometer. Fluorescence experiments were carried out on a QuantaMaster™ 40 Intensity Based spectrofluorometer from PTI technologies in the steady-state mode. Lifetime fluorescence was recorded using a DeltaFlex™ equipped with a picosecond photon detection module (PRO 850) and NanoLED laser source (300 nm with the emission set to 530 or 590 nm). X-Ray single crystal analysis and data collection were carried out at the University of Louisiana using a Bruker APEX2; cell refinement: Bruker SAINT; data reduction Bruker SAINT; program(s) used to solve structure: SHELX9<sup>39</sup> program(s) used to refine structure: SHELXL2013<sup>40</sup> molecular graphics were generated using the program X-Seed.<sup>41</sup>

### NMR experiments

A 20 mmol·dm<sup>-3</sup> solution of chemodosimeter **4a** was prepared by dissolving 5.1 mg in DMSO-*d*<sub>6</sub> (0.6 mL). To subsequently form the ketoximate (**4a**) in situ Hunig's base was added in slight excess. The following stock concentrations of the analytes of interest were prepared as follows; A 101 mmol·dm<sup>-3</sup> concentration of KCN in DMSO-*d*<sub>6</sub> was made, of which 236 μmol·dm<sup>-3</sup> (two equivalence) of KCN solution was added to the ketoximate (**4a**) directly in the NMR tube. Three equivalence (5.4 μL) of DECP was added directly into the NMR tube that contains the ketoximate (**4a**). The NMR spectrum were run within minutes of the sample being prepared. <sup>31</sup>P NMR: One equivalent (1.8 μL) of P<sub>4</sub>-*t*-Bu base was added to **4a** in the NMR tube. A triphenyl phosphite internal standard (375 mg·mL<sup>-1</sup>) was prepared in a capillary tube and inserted into the NMR tube. All the solvent were degassed by purging N<sub>2</sub>-gas before using.

### UV-Vis spectroscopy

A stock solution of **4a** (2.6 mmol·dm<sup>-3</sup>) or **4b** (2.5 mmol·dm<sup>-3</sup>) was prepared by dissolving 11.0 mg in DMSO (10,0 mL). A 16 μmol·dm<sup>-3</sup> solution (2 mL) of **4a** or **4b** was prepared from the stock solution in a 4 mL quartz cell for the UV-vis spectroscopic studies. A stock solution (1.6 mmol·dm<sup>-3</sup>) of analytes (DECP, DICP, DMMP, KCN) were also prepared in DMSO. Aliquots of the analytes (4 μL ≡ 0.2 equivalents of the analyte) was added to the UV-vis cell. The DMSO solvent was degassed by purging the solution with N<sub>2</sub>-gas before preparing solutions.

### Steady-state fluorescence spectroscopy

Stock solutions of **4a** and **4b** were prepared (2.5 mmol·dm<sup>-3</sup>) and used in the UV-vis, steady-state fluorescence, and lifetime studies. Hardware conditions for steady state fluorescence are as follows; λ = 336 nm, emission range = 345-640 nm or λ = 410 nm, emission range = 440-750 nm or both; slit width was 0.40 mm.

### Mass spectrometry

A stock solution of **4a** (0.5 mmol·dm<sup>-3</sup>) was prepared by dissolving 1.1 mg of **4a** in spectroscopic grade methanol:dichloromethane (4:1) mixture (5 mL) and injected into the ESI-MS. A second ESI-MS experiment was carried out by preparing a 1 mL volume of the stock solution of **4a** (0.5 mmol·dm<sup>-3</sup>) plus a 10 μL volume of KCN (101 mmol·dm<sup>-3</sup>) in an Eppendorf tube. In a third experiment a 1 mL volume of the stock solution of **4a** (0.5 mmol·dm<sup>-3</sup>), Verkade's base, 1 μL (12 equivalents) and fresh DECP was prepared in an Eppendorf tube immediately injected in the ESI-MS

### Molecular modelling

Models of the *E*-(*keto*) enamine-*anti*-ketoximate, the tabun mimic diethyl cyanophosphonate and the reaction product were generated using *Spartan* '20.<sup>8</sup> The lowest energy structures were determined by molecular mechanics using the Merck Molecular Force Field (MMFF). Geometries were refined by DFT methods (ωB97X-D/6-31G\*) and the energies recorded. The *Spartan* Transition State tool was used to generate a provisional transition state geometry for the ketoximate

reaction with diethyl cyanophosphonate (DECP) followed by the subsequent reaction of cyanide with the imine  $\alpha$ -carbon and the transition state energies calculated.

### Synthesis of 3-bis(propylamino)phenol (1).<sup>42</sup>

3-Aminophenol (3.3 g, 30 mmol), Na<sub>2</sub>CO<sub>3</sub> (4.8 g, 45 mmol), and 1-bromoalkane (8.1 g, 66 mmol) was added to a 1:1 mixture of iso-propanol: H<sub>2</sub>O (30 mL) and heated under reflux for 15 hrs. The solvent was evaporated by reduced pressure. The oily crude product was redissolved in a minimum amount of ethyl acetate and stirred for a further 2 hrs. The organic layer was extracted with saturated NaHCO<sub>3</sub> (3×30 mL), washed with H<sub>2</sub>O (3×30 mL), brine (3×25 mL) and H<sub>2</sub>O (3×25 mL). The organic layer then dried over Na<sub>2</sub>SO<sub>4</sub>, filtered and the solvent was removed under reduced pressure. The oil was subjected to silica column chromatography (60-200 $\mu$ m, 60 Å) using hexane:ethyl acetate (7:3) as the eluent. 3-Bis(propylamino)phenol (1) was obtained as a brown oil. Yield 3.5g, 18.1 mmol, 66%. <sup>1</sup>H-NMR (400 MHz, DMSO-*d*<sub>6</sub>):  $\delta$  8.95 (s, 1H), 6.88 (t, *J* = 8.0 Hz, 1H), 6.09 - 6.00 (m, 2H), 5.97 (d, *J* = 8.1 Hz, 1H), 1.51 (sx, *J* = 7.5 Hz, 4H), 0.86 (t, *J* = 7.4 Hz, 6H); <sup>13</sup>C NMR (100 MHz, CDCl<sub>3</sub>): 158.7, 149.7, 130.1, 103.4, 102.8, 99.0, 52.5, 20.5, 11.7; consistent with prior literature.<sup>42</sup>

### Synthesis of 7-bis(propylamino)-4-hydroxycoumarin (2).<sup>32</sup>

3-Bis(propylamino)phenol (1) (3.86 g, 20.0 mmol) was added to a solution of anhydrous toluene (50 mL) and magic malonate [bis-(2,4,6-trichlorophenyl)malonate; synthesized based on prior literature]<sup>22</sup> (9.26 g, 20.0 mmol). The reaction mixture was heated under reflux for 3 hrs. with constant stirring. The reaction mixture was cooled to room temperature; a gray ppt formed which was collected by filtration and washed with cold toluene (30 mL). Yield 3.35g, 12.8 mmol, 64%. <sup>1</sup>H-NMR (400 MHz, DMSO-*d*<sub>6</sub>):  $\delta$  7.54 (d, *J* = 8.9 Hz, 1H), 6.64 (dd, *J* = 2.1, 9.0 Hz, 1H), 6.41 (d, *J* = 1.8 Hz, 1H), 5.20 (s, 1H), 3.29 (t, *J* = 7.6 Hz, 6H), 1.55 (sx, *J* = 7.5 Hz, 4H), 0.90 (t, *J* = 7.3 Hz, 6H); <sup>13</sup>C NMR (100 MHz, CDCl<sub>3</sub>): 167.5, 163.5, 156.5, 151.7, 124.6, 108.7, 104.3, 97.0, 86.4, 52.3, 20.4, 11.5. Elemental analysis (%) calculated for C<sub>15</sub>H<sub>19</sub>NO<sub>3</sub>: C, 68.94; H, 7.33; N, 5.36; Recalculated for solvent H<sub>2</sub>O C<sub>15</sub>H<sub>20.06</sub>NO<sub>3</sub>: C, 66.51; H, 7.46 N, 5.17; Found for C<sub>15</sub>H<sub>20.06</sub>NO<sub>3</sub>: C, 66.21; H, 7.04 N, 5.17. HRMS observed for [C<sub>15</sub>H<sub>19</sub>NO<sub>3</sub>+Na]<sup>+</sup> = 284.1253; Calculated for [C<sub>15</sub>H<sub>19</sub>NO<sub>3</sub>+Na]<sup>+</sup> = 284.1257.

### General synthesis of coumarin-enamine derivatives molecular probes 4a and 4b.<sup>28</sup>

7-Bis(propylamino)-4-hydroxycoumarin (2) (1.0 mmol), and the appropriate primary amine (3a or 3b 1.0 mmol)<sup>28</sup> and triethyl orthoformate (1.5 mmol) was heated under reflux in iso-propanol (7.0 mL) with constant stirring for 15 hrs. Reaction mixture was allowed to cool at room temperature, a yellow ppt formed which was filtered and washed with cold iso-propanol (10 mL). Typical yields 80-88%.

**Characterization of 4a:** Yield 369.2 mg, 0.88 mmol, 88% yield; <sup>1</sup>H-NMR (600 MHz, DMSO-*d*<sub>6</sub>) and <sup>13</sup>C NMR (150 MHz, DMSO-*d*<sub>6</sub>): See supporting information table S1 and figures S1-S15 for 1D and 2D spectrum. LRMS ESI-MS: *m/z* for [M + H]<sup>+</sup> = 422.3; IR (ATR solid): 3264 (br)  $\nu_{\text{OH(oxime)}}$ , 3049 (m)  $\nu_{\text{C=C(enamine)}}$ , 2958 (m)  $\nu_{\text{CH}}$ , 1716 (s)  $\nu_{\text{CO}}$  (delta lactone), 1588 (s)  $\nu_{\text{CO}}$  (ketone) cm<sup>-1</sup>; HRMS ESI-MS observed for [C<sub>24</sub>H<sub>27</sub>N<sub>3</sub>O<sub>4</sub>+H]<sup>+</sup> = 422.2073; Calculated for [C<sub>24</sub>H<sub>27</sub>N<sub>3</sub>O<sub>4</sub>+H]<sup>+</sup> = 422.2074.

**Characterization of 4b:** Yield 349.1 mg, 0.80 mmol, 80% yield; <sup>1</sup>H-NMR (400 MHz, DMSO-*d*<sub>6</sub>), assignment of major *E*-(*keto*) enamine isomer:  $\delta$  13.52 (d, *J* = 13.4 Hz, 1H, NH), 8.77 (d, *J* = 13.3 Hz, 1H, CH<sub>enamine</sub>), 7.76-7.69 (m, 3H, CH<sub>aromatic</sub> and CH<sub>coumarin</sub>), 7.64-7.57 (m, 2H, CH<sub>aromatic</sub>), 6.66 (dd, *J* = 9.1 Hz, *J* = 2.4 Hz, 1H, CH<sub>coumarin</sub>), 6.36 (d, *J* = 2.2 Hz, 1H, CH<sub>coumarin</sub>), 3.93 (s, 3H), 3.26 (m, 4H), 2.18 (s, 3H), 1.57 (sx, *J* = 4.5 Hz, 4H) 0.91 (t, *J* = 7.4 Hz, 6H); and <sup>13</sup>C NMR (100 MHz, DMSO-*d*<sub>6</sub>): 180.1, 163.5, 160.2, 157.1, 154.0, 153.9, 153.1, 139.5, 134.0, 127.5, 127.0, 120.5, 109.0, 98.0, 96.8, 62.0, 44.6, 12.8, 12.7, 12.6; LR ESI-MS: *m/z* for [M + H]<sup>+</sup> = 436.3; IR (ATR solid): 3052 (w)  $\nu_{\text{C=C(enamine)}}$ , 2960 (m)  $\nu_{\text{CH}}$ , 1714 (s)  $\nu_{\text{CO}}$  (delta lactone), 1584 (s)  $\nu_{\text{CO}}$  (ketone) cm<sup>-1</sup>; HRMS ESI-MS observed for [C<sub>25</sub>H<sub>29</sub>N<sub>3</sub>O<sub>4</sub>+Na]<sup>+</sup> = 458.2049; Calculated for [C<sub>25</sub>H<sub>29</sub>N<sub>3</sub>O<sub>4</sub>+Na]<sup>+</sup> = 458.2050.

### Author Contributions

RM carried out the experimental work and contributed to the editing of the manuscript. PJC performed the molecular modelling and contributed to editing the manuscript. FF solved the solid-state structure and KJW managed the project and wrote the manuscript.

Corresponding Author: [Karl J. Wallace](mailto:Karl.J.Wallace) Department of Chemistry and Biochemistry, University of Southern Mississippi, Hattiesburg, Mississippi, 39406 United States. [e-mail: karl.wallace@usm.edu](mailto:karl.wallace@usm.edu) ORCID 0000-0003-4541-7523

### Conflicts of interest

No conflicts of interest to declare.

### Acknowledgements

KJW would like to thank the Department of the Army US Army Engineer Research and Development Center ERDC (Contract W912HZ-19-2-0044).

### Notes and references

The synthetic details and full characterization are reported in the ESI. Crystals structure of **4a** (2108067) has been deposited into the CCDC; containing the supplementary crystallographic data for this paper. This data can be obtained via <https://www.ccdc.cam.ac.uk/> or by contacting The Cambridge Crystallographic Data Centre, 12 Union Road, Cambridge CB2 1EZ, UK; fax +44 1223 336033

- Crystal data for **4a** C<sub>24</sub>H<sub>27</sub>N<sub>3</sub>O<sub>4</sub>, M = 421.48, yellow needle, 0.240 × 0.030 × 0.010 mm<sup>3</sup>, triclinic, a = 5.1039(3), b = 14.0847(8), c = 15.9717(9) Å, α = 69.320(4), β = 87.965(5), γ = 80.713(4)°, space group P $\bar{1}$  (No. 2), V = 1059.81(11) Å<sup>3</sup>, Z = 2, D<sub>c</sub> = 1.321 g/cm<sup>3</sup>, F<sub>000</sub> = 448, Bruker Kappa APEX-II DUO, CuKα radiation, λ = 1.54184 Å, T = 90.0(5)K, 2θmax = 118.0°, 9299 reflections collected, 3045 unique (R<sub>int</sub> = 0.1199). Final S = 0.95, R<sub>1</sub> = 0.120, wR<sub>2</sub> = 0.236, R indices based on 1468 reflections with I > 2(I) (refinement on F<sup>2</sup>), parameters 288, restraints 0. Lp and absorption corrections applied, μ = 0.738 mm<sup>-1</sup>.
- S. K. Kim and J. L. Sessler, *Chem. Soc. Rev.*, 2010, **39**, 3784-3809.
  - Z. Kokan and M. J. Chmielewski, *J. Am. Chem. Soc.*, 2018, **140**, 16010-16014.
  - P.-E. Danjou, G. De Leener, D. Cornut, S. Moerkerke, S. Mameri, A. Lascaux, J. Wouters, A. Brugnara, B. Colasson and O. Reinaud, *J. Org. Chem.*, 2015, **80**, 5084-5091.
  - M. E. Amato, F. P. Ballistreri, S. D'Agata, A. Pappalardo, G. A. Tomaselli, R. M. Toscano and G. T. Sfrazzetto, *Eur. J. Org. Chem.*, 2011, 5674-5680.
  - M. Ciardi, A. Galán and P. Ballester, *J. Am. Chem. Soc.*, 2015, **137**, 2047-2055.
  - B. Hua, L. Shao, Z. Zhang, J. Liu and F. Huang, *J. Am. Chem. Soc.*, 2019, **141**, 15008-15012.
  - G. Michael, *J. Chem. Soc., Dalton Trans.*, 1992, 3235-3242.
  - I. Tabushi, Y. Kuroda and T. Mizutani, *J. Am. Chem. Soc.*, 1986, **108**, 4514-4518.
  - A. M. Costero Nieto, S. Gil Grau, M. Parra Alvarez, P. M. Mancini, R. Martínez Máñez, F. Sancenón and S. Royo, 2008.
  - A. Manna, K. Jana, N. Guchhait and S. Goswami, *New J. Chem.*, 2017, **41**, 6661-6666.
  - T. J. Dale and J. Rebek, *J. Am. Chem. Soc.*, 2006, **128**, 4500-4501.
  - S. S. Ali, A. Gangopadhyay, A. K. Pramanik, S. K. Samanta, U. N. Guria, S. Manna, and and A. K. Mahapatra, *Analyst*, 2018, **143**, 4171-4179.
  - R. Gotor, A. M. Costero, S. Gil, M. Parra, R. Martínez-Manez, and and F. Sancenon, *Chem. Eur. J.*, 2011, **17**, 11994 - 11997.
  - A. M. Costero, M. Parra, S. Gil, R. Gotor, P. M. Mancini, R. Martínez-Máñez, F. Sancenón and S. Royo, *Chem. - Asian J.*, 2010, **5**, 1573-1585.
  - R. Gotor, S. Royo, A. M. Costero, M. Parra, S. Gil, R. Martínez-Máñez and F. Sancenón, *Tetrahedron*, 2012, **68**, 8612-8616.
  - A. Barba-Bon, A. M. Costero, S. Gil, R. Martínez-Máñez, and and F. Sancenóna, *Org. Biomol. Chem.*, 2014, **12**, 8745-8751
  - A. Barba-Bon, A. M. Costero, S. Gil, A. Harriman and F. Sancenón, *Eur. J. Chem.*, 2014, **20**, 6339-6347.
  - S. K. Sheet, B. Sen and S. Khatua, *Inorg. Chem.*, 2019, **58**, 3635-3645.
  - S. Sarkar, and and R. Shunmugam, *Chem. Commun.*, 2014, **50**, 8511--8513.
  - T. N. Annisa, S.-H. Jung, M. Gupta, J. Y. Bae, J. M. Park and H.-i. Lee, *ACS Appl. Mater. Interfaces*, 2020, **12**, 11055-11062.
  - L. Zeng, H. Zeng, L. Jiang, S. Wang, J. Hou, and, Yoon and Y., *Anal. Chem.*, 2019, **91**, 12070-12076.
  - K. J. Wallace, R. I. Fagbemi, F. J. Folmer-Andersen, J. Morey, V. M. Lynth and E. V. Anslyn, *Chem. Commun.*, 2006, 3886-3888.
  - I. Walton, M. Davis, L. Munro, V. J. Catalano, P. J. Cragg, M. T. Huggins and K. J. Wallace, *Org. Lett.*, 2012, **14**, 2686-2689.
  - S. Dhiman, M. Ahmad, N. Singla, G. Kumar, P. Singh, V. Luxami, N. Kaur and S. Kumar, *Coord. Chem. Rev.*, 2020, **405**, 213138.
  - K. Kaur, R. Saini, A. Kumar, V. Luxami, N. Kaur, P. Singh and S. Kumar, *Coord. Chem. Rev.*, 2012, **256**, 1992-2028.
  - X. Guo, C.-X. Liu, Y. Lu, Y.-W. Wang and Y. Peng, *Molecules*, 2022, **27**, 489.
  - M. C. Etter, J. C. MacDonald and J. Bernstein, *Acta Crystallogr., Sect. B: Struct. Sci.*, 1990, **46**, 256-262.
  - R. Mia, P. J. Cragg and K. J. Wallace, *J. Lumin.*, 2021, **235**, 118053.
  - G. Kumar, K. Paul and V. Luxami, *New J. Chem.*, 2020, **44**, 12866-12874.
  - S. Tshepelevitsh, A. Kütt, M. Lökov, I. Kaljurand, J. Saame, A. Heering, P. G. Plieger, R. Vianello and I. Leito, *Eur. J. Org. Chem.*, 2019, **2019**, 6735-6748.
  - A. M. Kelly-Rowley, V. M. Lynch and E. V. Anslyn, *J. Am. Chem. Soc.*, 1995, **117**, 3438-3447.
  - A. B. Davis, R. E. Lambert, F. R. Fronczek, P. J. Cragg and K. J. Wallace, *New J. Chem.*, 2014, **38**, 4678-4683.
  - K. J. Wallace, R. I. Fagbemi, F. J. Folmer-Andersen, J. Morey, V. M. Lynth and E. V. and Anslyn, *Chem. Commun.*, 2006, 3886-3888.
  - P. Gans, *Journal*, 2014.
  - N. M. o. A. Methods, *Journal*, 1994, **V 4**, 2-4.
  - E. Raber, A. Jin, K. Noonan, R. McGuire and R. D. Kirvel, *Int. J. Environ.*, 2001, **11**, 128-148.
  - Y. Kim, Y. J. Jang, S. V. Mulay, T. T. Nguyen, and and D. G. Churchill, *Chem. Eur. J.*, 2017, **23**, 7785-7790.
  - Y. J. Jang, O. G. Tsay, D. P. Murale, J. A. Jeong, A. Segev, and and D. G. Churchill, *Chem. Commun.*, 2014, **50**.
  - G. M. Sheldrick, *Acta Crystallogr., Sect A*, 2008, **64**, 112.
  - G. M. Sheldrick, *Acta Crystallogr., Sect C*, 2015, **71**, 3-8.
  - L. J. Barbour, *J. Supramol. Chem.*, 2001, **1**, 189-191.
  - J.-F. Ge, C. Arai, M. Kaiser, S. Wittlin, R. Brun and M. Ihara, *J. Med. Chem.*, 2008, **51**, 3654-3658.